Synthetic aperture adaptive optics concept

Theodore F. Zehnpfennig
Saul A. Rappaport
Andrew J. LePage

Visidyne, Inc., 10 Corporate Place
South Bedford Street, Burlington, MA 01803

ABSTRACT

A serious impediment to the development of large aperture adaptive optics systems for correction of atmospheric turbulence is the very large number of wavefront correction subsystems (each consisting of an actuator, an actuator drive circuit, and a wavefront measurement element) which are required, and the attendant cost of these subsystems. If wavefront correction is to be applied to a fully-filled circular pupil several meters in diameter, several thousand of these subsystems may be needed. This situation could, however, be ameliorated if the pupil were not fully-filled. Here, we demonstrate that the diffraction-limited resolution of a full circular pupil can be approached or equalled with a synthetic aperture optical system consisting of an elongated pupil which rotates. Separate exposures of the object scene are made at each of several rotational positions of the pupil, and the final scene is reconstructed from these exposures. No optical phase information is needed for the image reconstruction. The polished area corresponding to the elongated pupil could be an order of magnitude smaller than that of the full pupil, and thus the number of adaptive optics subsystems could be decreased by a similar factor. The technique does not allow us to reach the same limiting magnitude as does the full, diffraction-limited pupil. However, on somewhat brighter objects, it could achieve the angular resolution of the full pupil without the complication and cost of adaptively correcting the entire pupil.

1. INTRODUCTION

This paper describes a concept for a synthetic aperture telescope which is capable of yielding the angular resolution of a fully-filled circular pupil, but which uses a single elongated pupil whose area is approximately an order of magnitude smaller than that of the full pupil. The concept is illustrated in Fig. 1. The primary mirror consists of a long, narrow slice across the

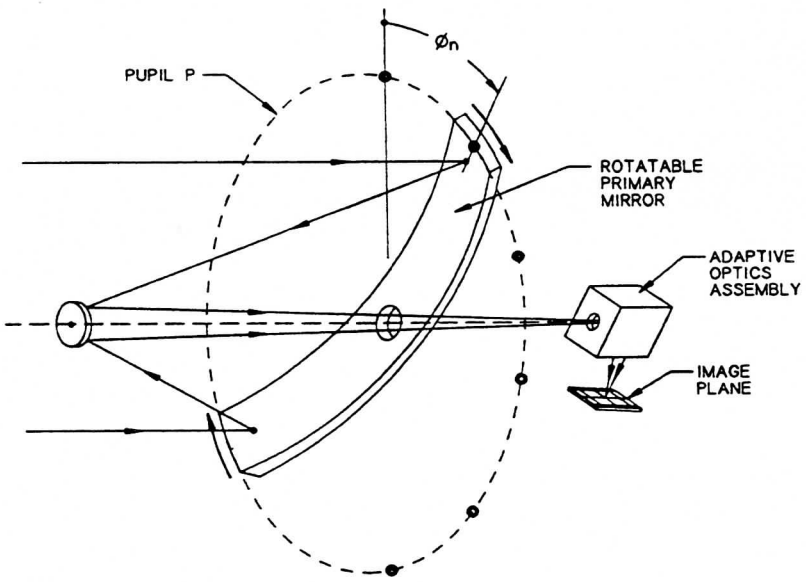

Fig. 1. The elongated pupil concept.

0-8194-1496-4/94/$6.00

diameter of the pupil P to be synthesized. In operation, the primary mirror is rotated about the optical axis, stepping through a sequence of angular positions ϕ_n, as shown. At each of these positions, a sub-exposure of the object scene is recorded. An algorithm operating on this set of sub-exposures is then used to reconstruct the final scene. The elongated pupil concept facilitates the implementation of adaptive optics techniques for correction of atmospheric turbulence because the polished area of the primary mirror is only a fraction of the area of the pupil P. Therefore, the number of adaptive optics components (actuators, actuator drive circuits, wavefront measurement subsystems, etc.) can be reduced by a similar fraction. The concept could also permit development of light-weight optics with high angular resolution for space applications.

Synthetic aperture configurations which are essentially linear have been proposed in the past. Among these are the SIMURIS instrument[1], the JPL Orbiting Stellar Interferometer[2], and the COSMIC linear optical array[3]. These instruments utilize linear arrays of separated, discrete sub-telescopes, the outputs of which are relayed to a central location and combined to form a final image. Relaying the radiation involves considerable optical complexity, and is particularly daunting since optical path length errors must be kept below $\lambda/10$. Accurate "phasing" of instruments of this type is a problem which has not yet been fully solved.

For synthesis of very large pupils (10 m to 100 m), use of telescope arrays such as the above devices will probably be necessary. However, for pupils of intermediate size (1 m to 10 m), the optical complexity and phasing problems of telescope arrays can be avoided. This is the purpose of the proposed concept, in which radiation collected over the active part of the pupil is combined directly onto the image surface, without use of complex relay optics, co-phasing systems, beam combiners, and elaborate internal metrology systems. (Here, the active part of the pupil is defined as that part occupied at a given time by the elongated primary mirror.) It is true that optical path length errors over the active pupil must still be kept below $\lambda/10$. However, this is a problem which has already been solved, as it is with any large astronomical telescope.

Because of the elongated, slit-like pupil employed here, this concept has been named the "Cat's Eye Imager".

2. IMAGE RECONSTRUCTION

The problem of image reconstruction with the Cat's Eye Imager is related to that of the reconstruction of tomographic data. As with tomography, each sub-exposure has a high resolution direction and, orthogonal to it, a low resolution direction, and these directions rotate around the axis of symmetry from sub-exposure to sub-exposure.

2.1 Reconstruction Algorithm

Let the set of sub-exposures $I_n(x,y)$ be recorded at N equally spaced angular positions over the range $\phi = 0°$ to $\phi = 180° \times (1\text{-}1/N)$, where ϕ is the orientation angle of the elongated pupil, and x and y are the image plane coordinates. Thus, for N = 16, ϕ ranges from 0° to 168.75°, in steps of 11.25°.

The $I_n(x,y)$ sub-exposures are then Fourier transformed, to give the set $\tilde{I}_n(k_x, k_y)$, where k_x and k_y are the coordinates in the Fourier plane. These are then multiplied by a weighting function $W(k_x, k_y)$, and summed:

$$J(k_x, k_y) = \sum_n \tilde{I}_n(k_x, k_y)\, W(k_x, k_y) \; . \qquad (1)$$

Finally, this sum is inverse Fourier transformed to produce the reconstructed image I_R:

$$I_R(x, y) = \tilde{J}\,(k_x, k_y) \; . \qquad (2)$$

The purpose of the weighting function $W(k_x, k_y)$, is to compensate for over-sampling of the central region of the Fourier plane. Figure 2 shows the MTF of the elongated pupil positioned on the Fourier plane. As the pupil is stepped through the N

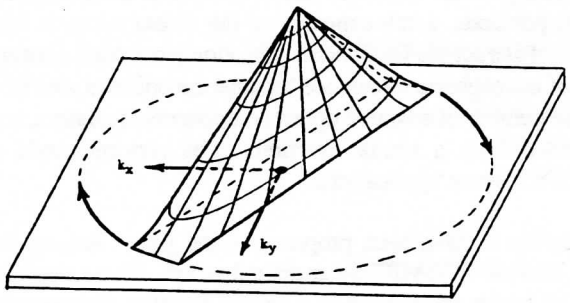

Fig. 2. General form of the elongated pupil MTF. The Fourier plane is sampled with one simple rotational motion.

angular orientations, the MTF rotates along with it. Thus, the central region of the Fourier plane, containing the lower spatial frequencies, is sampled during every sub-exposure, whereas the outer regions near the optical cutoff are typically sampled only once. $W(k_x, k_y)$ is used to correct this problem, which would otherwise degrade the angular resolution.

Figure 2 also illustrates how, with this image synthesis technique, the entire Fourier plane out to the cutoff frequency is sampled with one simple rotational motion.

2.2 Point Spread Function Calculations

The diffraction limited point spread function (PSF) for a single orientation of the elongated pupil is just the Fraunhofer diffraction pattern of a rectangular opening of size $s \times w$, and is given by:

$$P(\theta_x, \theta_y) = sin^2\ (\pi k_{ox}\theta_x)\ sin^2(\pi k_{oy}\theta_y)/[(\pi k_{ox}\theta_x)^2\ (\pi k_{oy}\theta_y)^2]\ , \qquad (3)$$

where θ_x and θ_y are the field angles, and $k_{ox} = w/\lambda$ and $k_{oy} = s/\lambda$ are the cutoff frequencies in cycles per radian. This function is shown in Fig. 3(a) for a pupil aspect ratio $s/w = 6$.

To find the PSF for values of N greater than 1, the basic point spread function P was stepped to each of the N angular orientations ϕ_n, and this set of functions was then combined using the reconstruction algorithm. The results of the calculations for N = 4 and N = 16 are shown in Figs. 3(b) and 3(c), respectively. The N = 4 PSF displays a prominent and nearly symmetrical central peak, surrounded by a substantial set of wings. In the N = 16 plot, the wings have been reduced to a considerably smaller set of rings. For comparison, the PSF of a full circular aperture of diameter s is shown in Fig. 3(d). The widths-at-half-height of (c) and (d) are seen to be comparable, with the reconstructed PSF in (c) perhaps being narrower by a few percent. Thus, for $N \approx 16$, we expect the imaging properties, for the elongated pupil technique after reconstruction, to be comparable to those of the fully-filled circular pupil.

For the above reconstructions, a very elementary type of weighting function was used. At each point k_x, k_y in the Fourier plane, the sum $\Sigma M_n (k_x, k_y)$ of the N modulation transfer functions was computed. If this sum was larger than unity, W was made equal to $1/\Sigma M_n (k_x, k_y)$. If, on the other hand, this sum was less than unity, the weighting function W was set equal to unity at that point. More sophisticated weighting functions should produce improved results, by for instance reducing the rings seen in Fig. 3(c).

2.3 Angular Tolerances and Registration

Must we take great care to insure that the rotation in the ϕ direction is extremely smooth and precise, and that only the very best bearings and encoders are used? Probably not. If the rotating assembly is locked or clamped in place for the period of each sub-exposure, mechanical play in the bearings is unimportant. This leaves pointing errors (in right ascension and declination, or in elevation and azimuth) due to bearing inaccuracies, and the error in ϕ due to encoder tolerances.

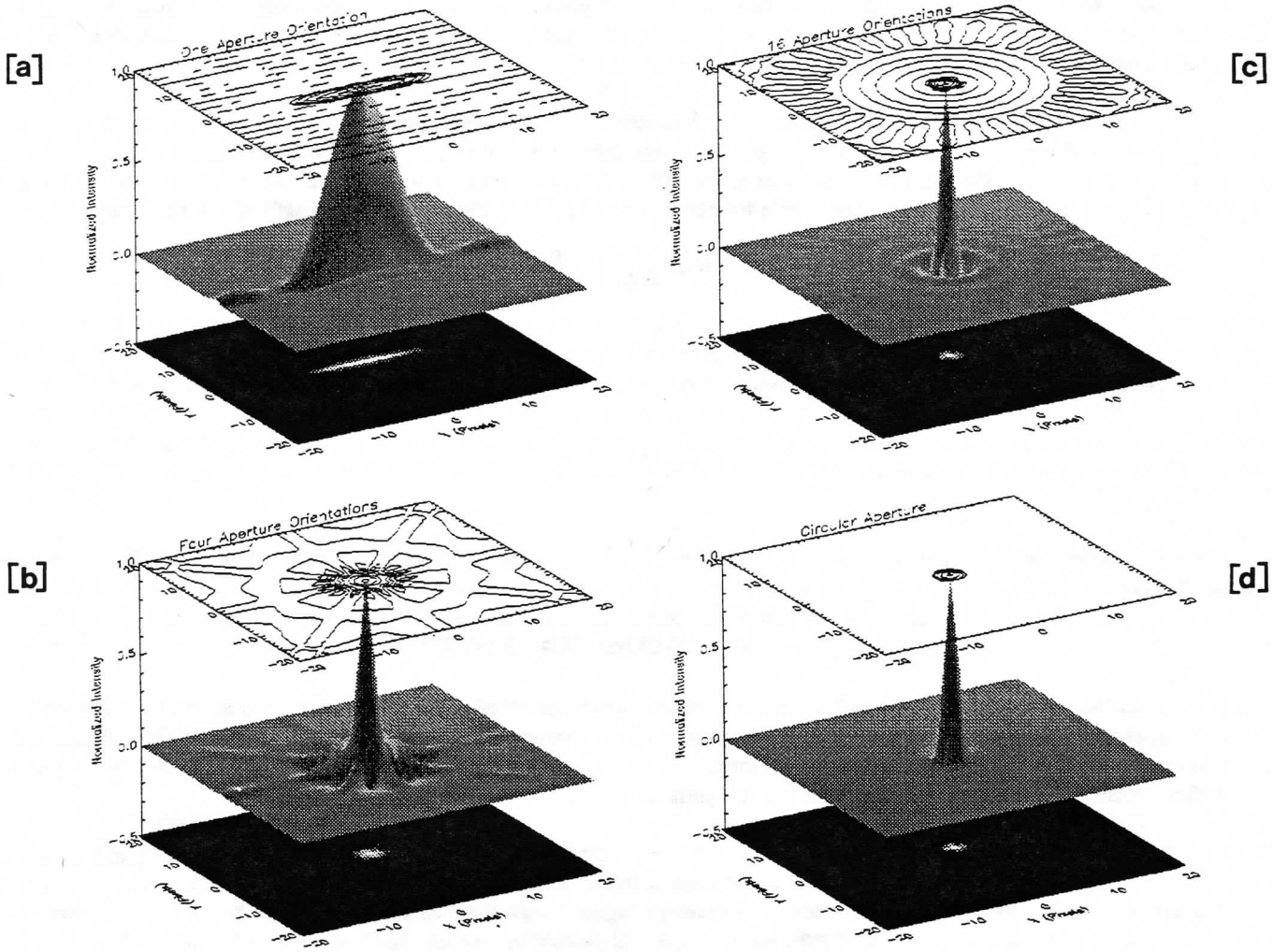

Fig. 3. Results of the point spread function calculations for one orientation (a), four orientations (b), sixteen orientations (c), and the full circular aperture (d).

Pointing errors will manifest themselves as registration errors from sub-exposure to sub-exposure during the reconstruction process. These errors can be minimized by accurate pointing and tracking while the sub-exposures are being taken, or by re-registration after the fact by means of cross-correlation techniques. In any case, there would be little point in trying to reduce these errors to less than 1/10 of a pixel or 1/10 of the diffraction limit. But this is the same tolerance which would be applied to any imaging system over the period of a time exposure. Thus, the rotation of the pupil does not impose additional constraints on the pointing tolerances.

As the pupil rotates in the ϕ direction, the elongated image of a point source in the field of view rotates along with it. See Fig. 4. The width β of this image is comparable to the diffraction limit. It should be sufficient, then, if the tolerance on ϕ is such that all parts of the image, including the parts furthest from the center of rotation, are correctly located in the focal plane to an accuracy of $\beta/10$. This corresponds to a tolerance on ϕ of $\beta/10$ divided by the half-length $\alpha/2$ of the image:

$$\Delta\phi = \frac{\beta}{5\alpha} . \tag{4}$$

However, the length-to-width ratio of the image α/β is equal to the aspect ratio s/w of the elongated pupil. Therefore:

$$\Delta\phi = \frac{w}{5s} . \tag{5}$$

For typical values of s/w in the range 6 to 15, the resulting value of $\Delta\phi$ ranges from 1.9° to 0.8°. Thus, the tolerance on ϕ is not at all stringent.

3. THE COHERENCE ISSUE

In the classical synthetic aperture concept, radiation from an array of collectors positioned across the entrance pupil to be synthesized is directed to a central location by systems of relay optics. There, it is combined coherently (in real time and with near-zero optical path length difference) before impinging on the detector or detector array. This phasing requirement is the most difficult technical problem associated with use of synthetic aperture techniques.

With the elongated pupil concept proposed here, radiation collected over the active area of the pupil is combined coherently to produce each sub-exposure. However, each sub-exposure, once recorded, exists as an intensity distribution only, and contains no information on the phases of the electromagnetic waves which formed it. The set of sub-exposures is then operated upon in the intensity domain by the reconstruction algorithm to produce the final scene. One might object that the use of phase information should be necessary for successfully combining the sub-exposures.

For an argument regarding this, see Fig. 5. In Fig. 5(a), a single spatial frequency component in the image is represented

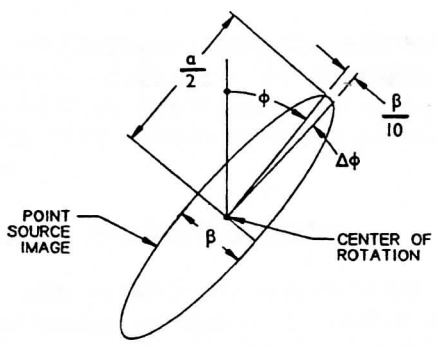

Fig. 4. Parameters for calculation of the tolerance $\Delta\phi$ on the angular position of the pupil.

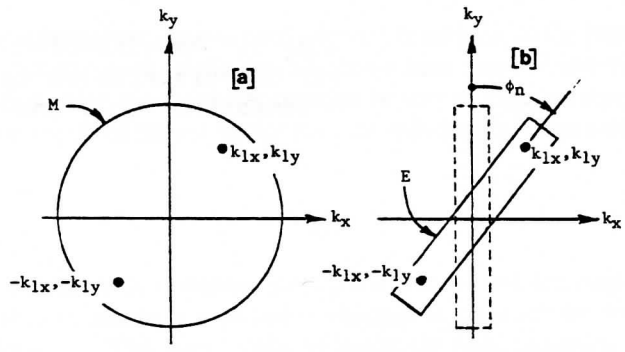

Fig. 5. Sampling of the Fourier plane with the MTF of a full circular pupil (a), and the MTF of an elongated pupil (b).

by the points k_{1x}, k_{1y} and $-k_{1x}$, $-k_{1y}$ on the Fourier plane. This spatial frequency is sampled by the circle M, which represents the MTF of a fully-filled circular aperture. The rectangle E in Fig. 5(b) represents the MTF corresponding to an elongated pupil whose length equals the diameter of the circular pupil. (The rectangle is the base of the pyramid-shaped figure seen in Fig. 2.) When the elongated pupil is rotated to an angular position near ϕ_n, as shown, it also will sample this spatial frequency component. The point is that the sampling of the component performed here is just as valid and complete as that done by the full circular pupil. The full image is then made up of a superposition of spatial frequency components sampled at various elongated-pupil orientations and properly combined using the reconstruction algorithm.

From an empirical point of view we note that, in the field of radio astronomy, data sets taken hours or days apart with telescope arrays such as the VLA are routinely combined as Fourier transforms of intensity domain information. Moreover, the PSF calculations of Section 2.2 and laboratory tests of Section 4 demonstrate explicitly that the technique does, in fact, work.

4. LABORATORY DEMONSTRATION

A simple laboratory test of a miniature version of the elongated pupil technique has been performed. The apparatus is illustrated in Fig. 6. A small telescope with an aperture of 90 mm and a focal length of 100 cm was focused on a test object located 4.5 meters from the telescope. Test objects consisted of photographic transparencies illuminated in transmission. An aperture mounting bracket for positioning various test apertures was located just in front of the telescope. The bracket was offset from the telescope axis, as shown, so that the test apertures would not overlap the secondary mirror of the telescope. The image formed by the telescope was recorded with a video camera, and selected video frames were digitized directly, using an 8-bit frame-grabber.

Three test apertures were used in this demonstration. The first was a circular opening 12.8 mm in diameter, and served as the fully-filled circular aperture. The second was a slit 0.91 mm wide with a length, 12.8 mm, equal to the diameter of the full circular aperture. This served as the elongated pupil aperture. Note that the length-to-width ratio of this pupil is 14. The third was a circular opening 3.85 mm in diameter, providing it an open area equal to the slit.

Test objects, consisting of photographic transparencies of various astronomical scenes, were placed in the test object plane, and images with different apertures in place were recorded. The elongated pupil aperture was stepped through 16 angular positions 11.25° apart, and an image was recorded at each position.

Results of the tests with transparencies of two objects, the galaxy NGC 2997 and the Crab Nebula, are shown in Figs. 7 and 8. Frame (a) in these figures shows the object through the fully-filled circular aperture. Frame (b) is one of the 16 sub-exposures through the elongated aperture, showing high resolution in one direction and lower resolution in the other. Frame (c) is the reconstructed image which results when the 16 sub-exposures are operated upon by the reconstruction algorithm. The weighting function used here is similar to that described in Section 2.2. The effectiveness of the technique and the fidelity of the reconstruction process can be determined by comparing the finer details seen in Frames (a) and (c). These frames do appear to be of comparable quality. For comparison, Frame (d) made through the equal area aperture shows what the scene looks like if the collecting area of the elongated pupil is re-arranged into a small fully-filled circular pupil. Note the substantially degraded resolution.

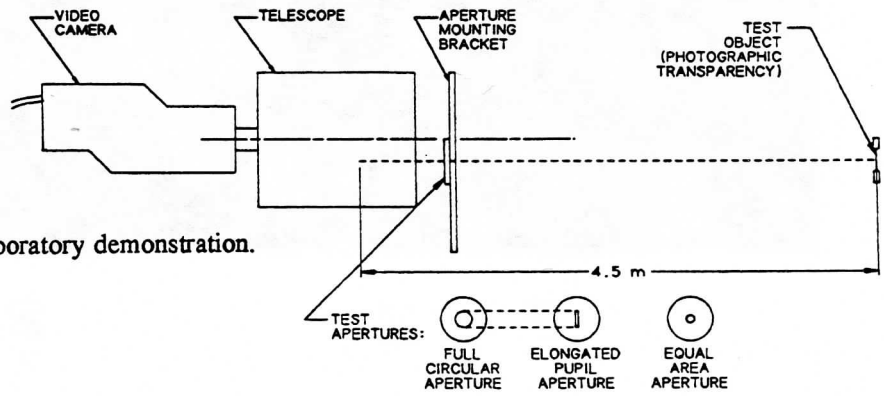

Fig. 6. Apparatus used for the laboratory demonstration.

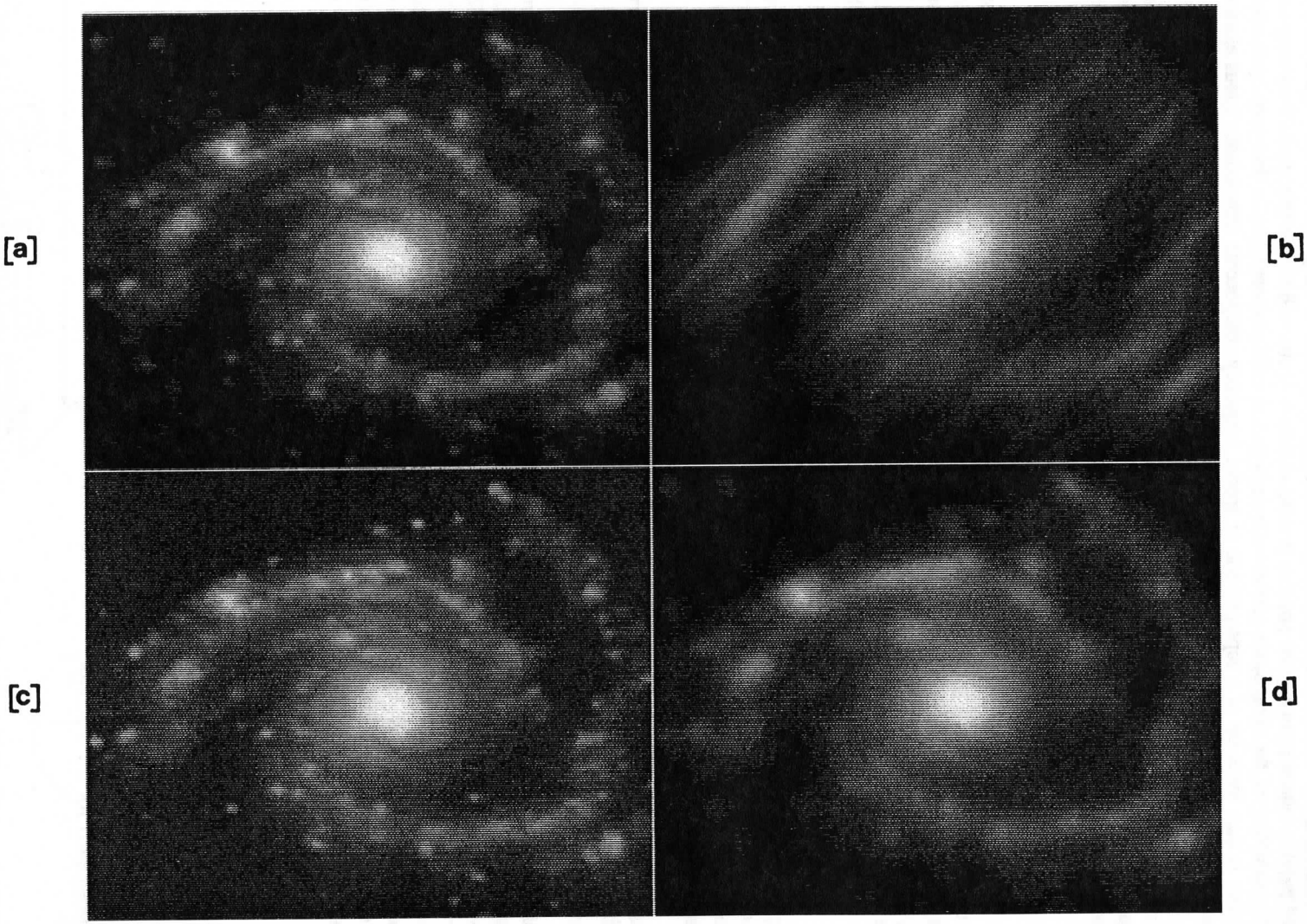

Fig. 7. Laboratory test using a transparency of NGC 2997: full circular aperture (a); one sub-exposure (b); reconstructed image (c); and equal-area aperture (d).

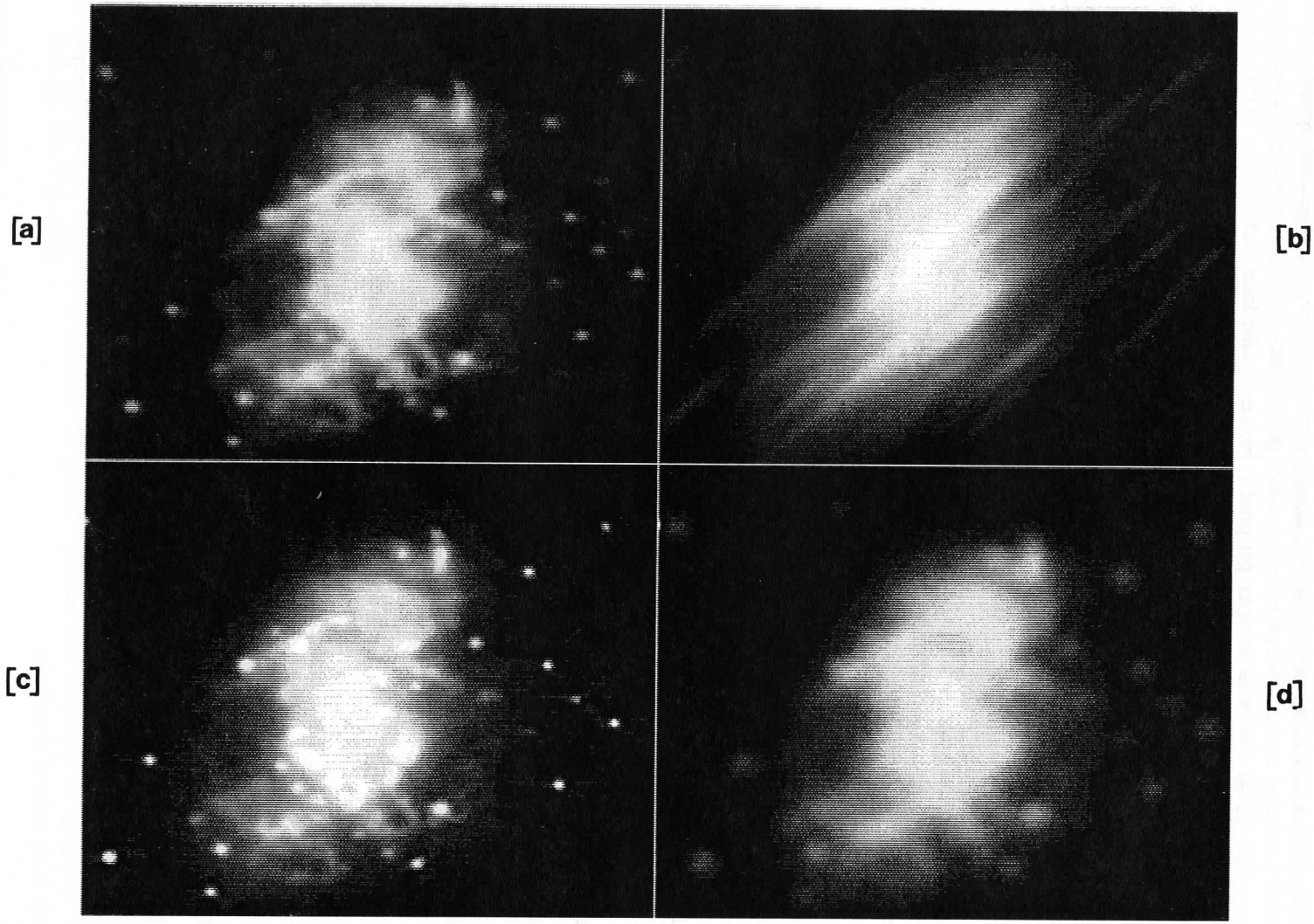

Fig 8. Laboratory test using a transparency of the Crab Nebula: full circular aperture (a); one sub-exposure (b); reconstructed image (c); and equal-area aperture (d).

5. SIGNAL-TO-NOISE CONSIDERATIONS

The signal-to-noise ratio (S/N) will be affected by the fact that, with this technique, the image of each object point in the sub-exposures falls upon an area of the detector several times larger than that for a conventional system. This fact can potentially affect the S/N because of increases in dark current, readout noise, and sky background over this now-larger image area. (Alternatively, we may view this as a decrease in signal per pixel.) Increased noise from each of these sources will go as the square root of the factor by which the image area was increased, or by the square root of the pupil aspect ratio s/w. For a cooled detector operating in the visible, the dark current should, however, be negligible. (This is not necessarily true in the infrared.) The effects of the readout noise can be reduced or made negligible by increasing the signal by means of sufficiently long integration times. The sky background, if a problem, could possibly be dealt with by indirect methods such as spectral filtering.

One optical technique for improving the S/N is image compression in the direction of the width w of the pupil. Since this is the low resolution direction, the image could presumably be compressed by a factor approaching the pupil aspect ratio without loss of image details. One-dimensional compression could be accomplished with an anamorphic lens system positioned near the image plane.

Another potential source of noise, which could be called "reconstruction noise", may arise because the final signal level in a given pixel after image reconstruction depends on the signal levels in many nearby pixels in the set of sub-exposures. Statistical fluctuations in these intensity levels and the effects of detector pattern noise would impact on the reconstructed level assigned to that given pixel.

These various sources of noise are quite dependent on the instrument design parameters, and further study using specific system designs are needed in order to quantify them.

6. APPLICATIONS

This section briefly describes some imaging systems in which the elongated pupil technique could be utilized.

6.1 Small Elongated Pupil Telescope

For good adaptive optics correction, the size of the sub-apertures within the entrance pupil should be no larger than r_o, the atmospheric turbulence coherence length[4]. Typically r_o ranges from 5 to 15 cm in the visible region. Let us choose an intermediate value of 8 cm for the size of the sub-apertures. Then, a reasonable minimum size for the primary mirror for an elongated pupil imager would be one sub-aperture wide by 10 to 15 sub-apertures long. Let us make it 8 cm by 96 cm, giving it the same collecting area as a 31.3 cm diameter circular pupil.

Let us arrange the actuators which control the shape of the deformable mirror in two rows of 13, spaced apart by a distance corresponding to the sub-aperture size. Thus, the system contains only 26 actuators. If, however, it can be made to operate at the diffraction limit, it will have an angular resolution λ/D of 0.12 arcsec in the visible. This is at least 4× better than a conventional telescope under the best seeing conditions, and is equivalent to a fully-filled 96 cm adaptive optics telescope requiring at least 130 actuators. Characteristics of this telescope are listed in Table 1.

6.2 Large Elongated Pupil Telescope

Consider a large 8 m elongated pupil telescope with 8 × 8 cm sub-apertures. Let the mirror width be 56 cm, giving a pupil aspect ratio of 14.3. The collecting area here is equivalent to a 2.4 m circular pupil. If we project the sub-aperture grid onto the deformable mirror and place one actuator at each intersection point of the grid, the total number of actuators required is 101 × 8 = 808. In contrast, a fully-filled 8 m telescope having sub-apertures of the same size would require about 8000 actuators, an increase of an order of magnitude.

Adaptive optics systems may utilize artificial laser beacons for measurement of the wavefront distortion. Large aperture systems may require multiple beacons in order to reduce the wavefront measurement errors due to focus anisoplanatism[5]. An elongated pupil telescope such as this has the advantage of requiring fewer beacons than a full-pupil telescope of the same

4. D. Greenwood and C. Primmerman, "Adaptive Optics Research at Lincoln Laboratory", Lincoln Laboratory Journal 5, 3-23 (1992).

5. J. Beckers, "Adaptive Optics for Astronomy: Principles, Performance, and Applications", Ann. Rev. of Astron. and Astrophys. 31, (1993).

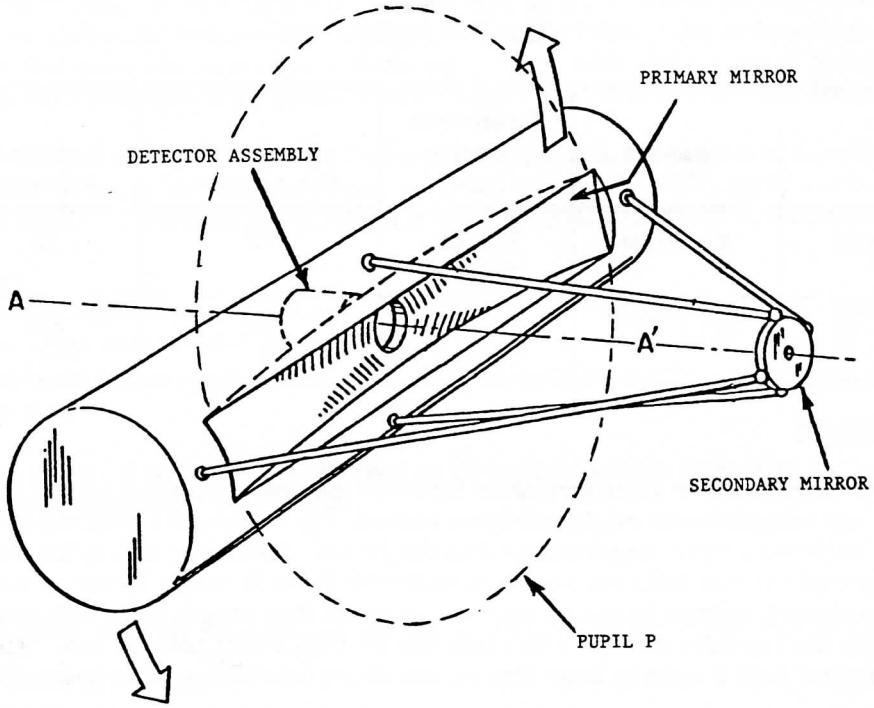

Fig. 9. A large, space-based elongated pupil telescope.